Total cross sections for the scattering of low-energy electrons by excited sodium atoms in the $3\,^2P_{3/2}$, $m_J = \pm 3/2$ state

B. Jaduszliwer, R. Dang,* P. Weiss, and B. Bederson
Physics Department, New York University, New York, New York 10003
(Received 13 July 1979)

The authors have measured the absolute total cross section for low-energy electrons scattered by sodium atoms in the $3\,^2P_{3/2}$, $m_J = \pm 3/2$ state using a modified atomic-beam-recoil technique. A single-mode tunable dye laser is used to excite these states selectively, and their populations are determined by using the atomic recoil in resonant photon interactions to separate excited from nonexcited beams spatially. Total cross sections have been measured at seven electron energies between 0.84 and 6.0 eV.

I. INTRODUCTION

Current interest in collision experiments involving excited-state atoms is very high. Excited-state processes play a major, sometimes dominant, role in a vast variety of phenomena involving bulk gaseous and plasma systems. Even when the relative concentration of excited-state atoms is very small, collisions involving them can dominate, since excited-state cross sections are often orders of magnitude larger than those involving ground-state atoms. Nevertheless, until very recently collision experiments were performed almost exclusively with atomic systems in their electronic ground state. The main exceptions involved either experiments in which excited-state atoms were present because the collisions under study took place under conditions such as those existing in a gaseous discharge, or atomic beam experiments performed on metastable excited atoms.[1] Obvious difficulties prevented the performance of experiments involving short-lived excited states; atoms survive in these states for times of the order of 10^{-8} sec and, at thermal speeds, travel only about 10^{-3} cm during that time interval.

The advent of the cw single-mode tunable dye laser has made possible the creation of a substantial steady-state excited-atom population within the interaction region of an otherwise conventional crossed-beam experiment, thus opening the way for an increasing number of atom-atom[2,3] and electron-atom[4-6] collision experiments involving excited states of the target beam. In particular, Hertel and co-workers[4] have studied in detail the dependence of inelastic electron scattering by $3\,^2P_{3/2}$ sodium atoms on the plane of polarization of the laser light for $3p \rightarrow 3s$ and $3p \rightarrow 4s$ transitions, thus determining the (relative) scattering multipole moments T_0^2 and T_1^2.

The monochromaticity and well-defined polarization of the laser light allow us to specify completely the hyperfine state into which the atom is excited, making possible the detailed study of fine- or hyperfine-structure transitions, or transitions between substates of different azimuthal quantum numbers. Some theoretical aspects of these novel problems have been discussed by Macek and Hertel.[7] Much of the recent work in this rapidly growing area of atomic collisions physics has been summarized in a review by Hertel and Stoll.[8]

The availability and efficiency of suitable dyes determines which atoms are accessible to this type of experiment. Initially, experiments were restricted to rhodamine 6G, which has maximum efficiency at frequencies very close to those for the sodium $3S \rightarrow 3P$ transitions. Rapid progress in dye technology, as well as the availability of new ring lasers, will change this situation in the near future. But even in the absence of such technical restrictions, sodium would have been a good choice for a first excited-state atom-electron collision experiment.

There is an ever increasing body of both experimental and theoretical results for low-energy electron scattering on the alkali atoms in their ground states. Most of the experimental work has been performed with sodium and potassium and includes the measurement of total,[9-11] differential,[10,12-14] direct differential,[14] and exchange differential[10,15,16] elastic cross sections, as well as some differential n^2S-n^2P cross sections,[17,18] both with and without spin analysis. The characteristic feature of these experiments is the generally good agreement existing between measurements and the results of few-state close-coupling calculations,[19-21] although some discrepancies exist.[22] Moores *et al.*[23] have extended their four-state close-coupling calculations to the scattering of electrons by excited sodium atoms. Performing an excited-state experiment on sodium would provide an opportunity to check the validity of such an extension.

Our initial efforts in connection with excited-

state atom collisions have thus been directed towards obtaining reliable absolute cross sections for the scattering of electrons by sodium atoms in the $3\,^2P_{3/2}$ state. This work is part of a continuing program that includes measurements of state-selected and spin-analyzed total and differential cross sections for elastic, inelastic, and superelastic electron-excited sodium collisions. Preliminary results have been reported elsewhere.[5,24,25]

II. GENERAL DESCRIPTION OF METHOD

The natural lifetime of the $3\,^2P_{3/2}$ state of sodium is of the order of 10^{-8} sec. At thermal speeds such an atom will travel about 2×10^{-3} cm before decaying to the ground state. Accordingly, in order to observe electron collisions with the excited sodium atoms, it is necessary for the laser, atomic, and electron beams to overlap. The geometry of the interaction region which we have chosen for our experiments is shown in Fig. 1; the three beams intersect each other orthogonally.

In the absence of the laser beam this geometry is identical to that used in the atomic-recoil technique developed at New York University[26] for ground-state experiments. This technique has been described in detail elsewhere.[11,17] The main difference between this and other techniques is that observation is made on the recoiled atoms, rather than on the scattered electrons. The atomic-recoil angles are large enough to allow not only the determination of total scattering cross sections by measuring the attenuation of the atomic beam when cross-fired by electrons, but also the study of differential scattering by collecting atoms scattered away from the beam axis. The recoil technique is particularly amenable to the performance of scattering experiments with state selection before the interaction, and with state analysis after the interaction.

Figure 2 illustrates the relationships between the atomic-recoil angles ψ (in the xy plane, defined by the atomic and electron beams) and χ (in the yz plane), and the electron polar and azimuthal scattering angles θ and ϕ. These relationships are given by

$$\psi=\alpha-\beta\cos\theta\,, \tag{1}$$

$$\chi=\beta\sin\theta\sin\phi\,, \tag{2}$$

where $\alpha=mv/MV, \beta=mv'/MV$; mv and mv' are the magnitudes of the electron momentum before and after the collision, respectively, and MV is the magnitude of the atomic momentum assumed unchanged in the collision. If the collision is elastic, $\alpha=\beta$. It is assumed that α and β are small, although this restriction is not required for the present total cross section experiments.

To measure a total cross section σ, one performs a "scattering-out" experiment, measuring the difference between the atom current I_0 reaching the detector which is set on the atomic beam axis with the electron beam off, and the one with the electron beam on, I. The total cross section is related to the experimental parameters by

$$\sigma=(\Delta I/I_0)(Vh_A/I_e)\,, \tag{3}$$

where $\Delta I=I_0-I$, h_A is the height of the atomic beam, V is the atomic beam speed, and I_e is the electron current (electrons per second). It is important to stress that when using this method it is not necessary that one measure absolute atomic beam densities or currents; only the absolute electron current passing through the interaction region must be determined.

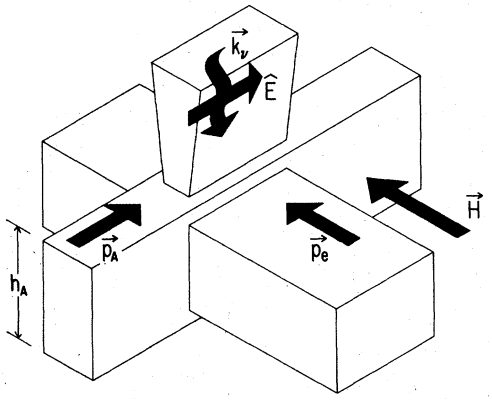

FIG. 1. Interaction region: $\vec{P}_A$, $\vec{P}_e$, and $\vec{k}_\nu$ are the atom, electron, and photon momenta; $\hat{E}$ gives the laser-beam polarization. The magnetic field $\vec{H}$ is 785 G parallel to the electron beam; h_A is the height of the atomic beam.

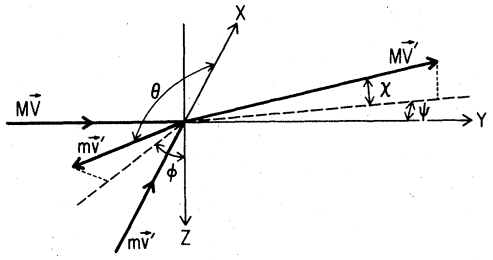

FIG. 2. Atomic recoil and electron scattering angles. The electron and atom beams define the x and y axes; the z axis completes a right-hand coordinate set. The usual electron polar and azimuthal scattering angles θ and ϕ are defined with respect to the x and z axes, respectively. The atomic recoil angles are ψ and χ; ψ is defined in the xy plane, χ in the yz plane.

When two atomic species of total electron scattering cross sections σ_1 and σ_2 are present, the observed "effective" total cross section $\bar{\sigma}$ will be given by

$$\bar{\sigma} = \mathfrak{F}\sigma_1 + (1 - \mathfrak{F})\sigma_2 , \tag{4}$$

where $\mathfrak{F}$ is the fraction of species-1 atoms present in the interaction region.

In our case species 1 would be the $3\,^2P_{3/2}$ sodium atoms, species 2 the ground-state sodium atoms, and $\mathfrak{F}$ the fraction of excited atoms present in the interaction region. We are assuming here that the excitation mechanism prepares a statistical mixture, rather than a coherent superposition, of atoms in the ground and excited states. This assumption is discussed in Sec. III.

III. ATOMIC EXCITATION

Figure 3 shows the hyperfine energy levels for the ground and $3\,^2P_{3/2}$ states of sodium in the presence of a 785-G magnetic field.[27] At this field strength the nuclear and magnetic moments are fully decoupled for the excited state, whereas for the ground state the atoms are in the intermediate-field regime, with the dimensionless Rabi parameter $x = g\mu_B H/\Delta W = 1.24$, where g is the gyromagnetic factor, μ_B is the Bohr magneton, H is the magnetic field intensity, and ΔW the zero-field hyperfine energy splitting. We use the quantum numbers (m_I, m_J) to describe the excited-state sublevels, while the ground-state ones are labeled (F, m).

The natural width of the transitions between the ground- and excited-state sublevels is of the order of 10 MHz, while the laser width is about 50 MHz, and for mutually perpendicular atomic and laser beams the Doppler broadening is, in principle, negligible. The average separation between $3\,^2P_{3/2}$ levels differing in one unit of m_J is 1460 MHz, while the splitting of levels of the same m_J, differing by one unit of m_I, is 30 (for $m_J = \pm\frac{3}{2}$) or 10 MHz (for $m_J = \pm\frac{1}{2}$). The separation between adjacent ground-state levels varies between 260 and 1220 MHz. It follows that it is possible, in principle, to resolve each of the different allowed transitions by proper frequency and polarization selection of the laser light.

It is well known that, because of the $\Delta m = \pm 1, 0$ selection rule for the decay of the excited state, optical pumping will deplete most of the ground-state hyperfine sublevels after a few excitation-deexcitation cycles. The exceptions are the $(2,2) \rightarrow (\frac{3}{2}, \frac{3}{2})$ and $(2,-2) \rightarrow (-\frac{3}{2}, -\frac{3}{2})$ transitions, denoted by arrows in Fig. 3. These are the ones that were used in our experiment to create an excited-state population in the interaction region.

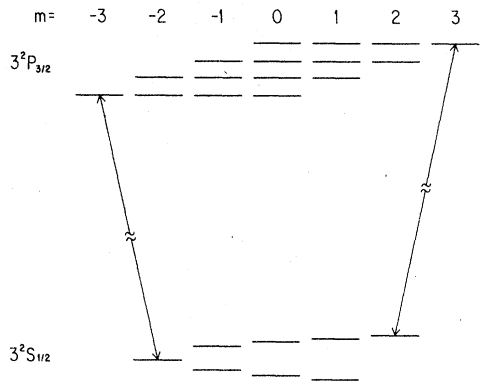

FIG. 3. Zeeman structure of the $3S_{1/2}$ and $3P_{3/2}$ states of sodium ($H = 785$ G). Ground-state levels (F,m) are (1,1), (1,0), (1,−1), (2,−2), (2,−1), (2,0), (2,1), and (2,2), beginning with the lowest one and moving clockwise. Excited-state levels (m_I, m_J) are ordered in columns of constant $m = m_I + m_J$ and rows of constant m_J, beginning with $m_J = \frac{3}{2}$ in the bottom row.

Thus under the conditions of our experiment we have an effective "two-level" system, with the excited atoms virtually exclusively in the $3\,^2P_{3/2}$, $m_J = \frac{3}{2}$ (or $-\frac{3}{2}$) magnetic sublevel.

The magnetic field present in the interaction region is parallel to the electron momentum and defines the quantization axis. To observe the $\Delta m = \pm 1$ transitions discussed in the preceding paragraph using linearly polarized laser light, we set the electric vector parallel to the atomic momentum, as shown in Fig. 1. When the laser is tuned to either one of the $(2, \pm 2) \rightarrow (\pm\frac{3}{2}, \pm\frac{3}{2})$ transitions, the atoms will exchange photons with the laser field during their entire passage through the interaction region.

For laser intensities which are not too high and linewidths which are not too narrow, perturbation theory is applicable, and one can write rate equations to describe the population dynamics of ground and excited states. Under these conditions the target atoms can be represented as an incoherent mixture, rather than as a coherent superposition, of atoms in the ground and excited states. Therefore Eq. (4) for the total observed cross section will be valid. This is not a moot question, since the description of the electron scattering process changes, depending on which target characterization one chooses, as has been discussed in detail by Gersten and Mittleman,[28] Mittleman,[29] and Hertel and Stoll.[8] We took the somewhat naive approach of assuming that, if the period of the Rabi oscillation of the atom in the radiation field is substantially longer than the lifetime of the excited state against spontaneous decay, there will not be significant coherence between ground and excited states. This is indeed

the case, given the parameters of our laser, and Eq. (4) can be used safely.[30] Mittleman[29] obtained equivalent results using the rotating-wave approximation.

The rate equations governing the excitation-deexcitation process in the interaction region are

$$f_0(t) = 1 - f_1(t)\,, \tag{5}$$

$$\dot{f}_1(t) + (1+2\rho)Af_1(t) = \rho A \tag{6}$$

where f_0 and f_1 are the populations of the ground and excited states, respectively; A is the Einstein coefficient associated with spontaneous emission of radiation, and $\rho = \lambda^3 P/8\pi hca\Delta\nu$ is the ratio of stimulated emission rate to spontaneous emission rate. P is the laser power, a is the laser-beam cross sectional area in the interaction region, and $\Delta\nu$ is the laser linewidth. The solution for f_1 with the initial condition $f_1(0) = 0$ is

$$f_1(t) = \{1 - \exp[-(1+2\rho)At]\}\rho/(1+2\rho)\,, \tag{7}$$

which for $t \to \infty$ gives a steady-state population f_1 of the excited state

$$f_1 = \rho/(1+2\rho)\,. \tag{8}$$

The atomic transit time $\tau = l/V$ through the interaction region of length l is of the order of 10^{-5} sec, while the characteristic excitation time $1/(1+2\rho)A$ is of the order of 10^{-8} sec. Under normal operating conditions each atom will undergo several hundred excitation-decay cycles, and the steady-state solution will describe the populations of both ground and excited states. The average time spent by each atom in the excited state while crossing the interaction region will be $\Delta t = f_1\tau$.

It should be noted that f_1 is the excited-state fraction relative to the population initially in the particular ground-state hyperfine sublevel being pumped by the laser. In general, since there are eight such sublevels in the sodium ground state, only 12.5% of the full atomic beam is available for excitation.

In order to determine, using Eq. (4), the total cross section for electron scattering by the excited sodium atoms, one must determine $\mathfrak{F}$. We will show that $\mathfrak{F} = f_1$ and will describe a method to determine $\mathfrak{F}$ taking advantage of the atomic recoil associated with the resonant photon interactions. Resonant many-photon recoil is readily observable in an atomic beam experiment.[31] In our geometry the downward momentum transfer per absorbed photon, Δp, results in a recoil angle $\gamma_0 = h/MV\lambda$, where λ is the photon wavelength. Stimulated emission of a photon results in an upward momentum transfer Δp to the atom and an opposite recoil angle γ_0, so that the net recoil for each such pair of events is zero. However, spontaneous-decay photons are radiated in essentially random directions, each such event again transferring Δp to the atom.

An atom which spends a total time Δt in the excited state will undergo an average number of spontaneous decays $N = \Delta t/\tau_0$ ($\Delta t \gg \tau_0$), where τ_0 is the natural lifetime of the excited state. The effect of these N spontaneous decays on the atomic momentum can be described as a three-dimensional random walk in momentum space, with uniform step size Δp. Neglecting the anisotropy in the angular distribution of spontaneous photons, in the first approximation the probability distribution function for a net momentum transfer $\vec{p}$ to the atom after N steps[32] is, for large N,

$$W(\vec{p}) = (\tfrac{2}{3}\pi N\Delta p^2)^{-3/2}\exp(-3p^2/2N\Delta p^2) \tag{9}$$

and the average momentum transfer is zero. The atom will suffer a net momentum transfer $N\Delta p$ from the absorbed photons, and the net downward recoil angle will be

$$\gamma = N\gamma_0 = f_1(h/MV\lambda)(\tau/\tau_0)\,. \tag{10}$$

In the limit of high laser power, the net recoil saturates at $\gamma_0\tau/2\tau_0$.

If the atomic detector is at a distance L from the interaction region, the deflection d of the atomic beam due to resonant photon interactions is

$$d = L\gamma = Lf_1(h/MV\lambda)(l/V\tau_0)\,. \tag{11}$$

By measuring d and using Eq. (11), we can determine f_1.

As has been discussed earlier in this section, only $\frac{1}{8}$ of the atomic beam (or $\frac{1}{4}$, if the beam has been polarized in high fields by a Stern-Gerlach magnet selecting a single value of m_J) participates in the excitation process. In our experimental arrangement, d is of the order of 0.2 in., whereas the height of the atomic beam, measured at the detector, is also about 0.2 in. (FWHM). This means that those atoms that were excited by the laser and have spent a fraction f_1 of the transit time through the interaction region in the $3\,^2P_{3/2}$ state are spatially separated from the ones that have not been excited. We can say that the atomic beam is split into two beams in the interaction region and that the beam which makes an angle γ with the axis of the apparatus is indeed an "excited-state beam."[33] Under these conditions, f_1 and $\mathfrak{F}$ are identical.

The spontaneous decays introduce two sources of random fluctuations in d: first, the number of spontaneous photons itself follows a Poisson distribution with mean N and variance N, and second, the variance in the momentum transferred to the atoms by the N spontaneous photons can be com-

puted from Eq. (9) to be $N\Delta p^2/2\pi$. The relative error in the determination of $\mathfrak{F}$ due to these two sources can be shown to be $[(2\pi+1)/2\pi N]^{1/2}$.

The spontaneous decays will also broaden the atomic beam. An estimate of the broadening can be obtained from the variance of the probability distribution [Eq. (9)]:

$$b \simeq (N/2\pi)^{1/2}(\Delta p/MV)L\,, \tag{12}$$

where b is the beam broadening.

We have thus far assumed that the only limitation on the number of photons absorbed per atom is the available laser power density. In fact, this is not the case. As the atom acquires momentum in the transverse direction, the laser photons become red shifted relative to the atom. Eventually the atom ceases to absorb photons. It is easy to calculate the Doppler shift per absorbed photon,

$$\Delta\nu = (\Delta p/Mc)\nu_0 \simeq 0.05 \text{ MHz}\,. \tag{13}$$

The average accumulated Doppler shift will be $N\Delta\nu$, and this number must be kept smaller than half the laser bandwidth; i.e., transverse recoil using our present arrangement limits N to less than 500.

IV. APPARATUS

As the atomic-beam apparatus used for this experiment has been discussed in detail previously,[10,11,15-18] we include here only a very brief description. Figure 4 shows a schema of our experimental arrangement.

A. Atomic beam

The sodium-beam source is an effusive oven constructed of iron, and is heated to a temperature of about 500 °C. The ground-state beam is polarized in high fields (selecting one of the two m_J values) by an offset Stern-Gerlach magnet, so that the number of hyperfine ground-state sublevels present in the atomic beam is four rather than eight. The magnet also acts as a velocity selector, giving a velocity spread $\Delta V/V \simeq 0.08$.

After passing through the interaction region, the atoms are surface ionized on a hot platinum wire. The ions are mass analyzed by a 60° sector magnet and detected by a Channeltron electron multiplier operated in the current mode, its output being monitored by an electrometer.

The distance between the interaction region and detector is $L = 32$ in. The detector can be moved vertically (z axis) and horizontally (x axis) to obtain a cross sectional intensity of the atomic beam, and can be aligned either on axis to monitor the full atomic beam or below axis to monitor the "excited" beam discussed in Sec. III.

B. Electron beam

The electron gun is similar to that described by Collins *et al.*[34] It lies between the pole pieces of a permanent magnet, producing a field of 785 G parallel to the electron momentum. The electron beam is shaped like a ribbon, about 1 in. wide and 0.032 in. high [the electron beam height must be kept smaller than the atomic beam height for Eq. (3) to be valid]. The electron current through the interaction region is monitored by a digital microammeter. Currents between 200 and 500 μA were used in the present experiment. The energy width of the electron beam is about 0.40 eV (FWHM); the mean electron energy is corrected for space-charge effects and contact potentials.

C. Atomic velocity determination

Equations (3) and (11) require the explicit measurement of the atomic beam velocity. This is accomplished by a technique described by Collins *et al.*[10] Electrons which are inelastically scattered in the forward direction ($\theta = 0$) result in recoiled atoms for which $\psi = \alpha - \beta$ [Eq. (1)] and $\chi = 0$ [Eq. (2)]. Because of the finite height of the detector, such atoms are detected with greater efficiency, i.e., have a very high "azimuthal form factor,"[10] compared to those for which $\theta > 0$, for which χ is not necessarily zero. Thus these $\theta = 0$ inelastically scattered electrons give rise to a peak in the atomic angular distribution as a function of detector position, as shown in Fig. 5.

The position of the forward inelastic scattered

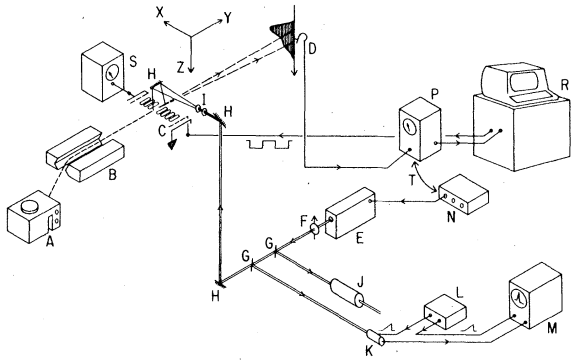

FIG. 4. Experimental arrangement: A sodium oven; B Stern-Gerlach magnet; C electron gun; D Channeltron electron multiplier; E tunable dye laser; F polarization rotator; G beam splitters; H mirrors; I lenses; J sodium vapor cell; K spectrum analyzer; L spectrum analyzer ramp generator; M mode structure monitoring scope; N tunable dye laser frequency control; P atomic-beam monitoring electrometer; R DECLAB-03 computer; S electron-beam monitoring microammeter; T laser-frequency manual feedback loop.

peak, s, is related to the electron energy E and atomic velocity V by

$$s = [(2m)^{1/2}/M]L[\sqrt{E} - (E - E^*)^{1/2}]/V, \qquad (14)$$

where E^* is the excitation energy. Thus, by measuring the displacement of the forward inelastic scattering peak, the average atomic beam velocity can be determined to better than 3%.

D. Laser beam

A single-mode tunable dye laser using rhodamine 6G as the lasing medium is pumped by a 1-W argon-ion laser. One can tune the laser frequency manually to the desired transition, using commercial piezoelectric drives for the cavity back mirror and an intracavity etalon. Coarse tuning of the resonant transition is accomplished by monitoring the fluorescence in a sodium vapor cell, while fine tuning of the particular hyperfine transition we are seeking is accomplished by monitoring the atomic beam itself, making use of the atomic recoil associated with resonant photon interactions. A spectrum analyzer is used to monitor the laser mode structure. A polarization rotator allows us to choose the desired polarization for the photon in the interaction region. A cylindrical lens stretches the laser beam along the atomic beam, so as to illuminate the full length of the interaction region. An auxiliary spherical lens helps to confine most of the power in the laser beam to the region of interest. The laser power in the interaction region is of the order of 0.1 W/cm^2.

E. Data acquisition and processing

The output of the atomic beam monitor electrometer is fed into the analog-to-digital converter of a DECLAB-03 computer which is programmed to sample repetitively the beam signal with the electron gun off, to turn the electron gun on and sample the signal again, and then to turn the electron gun off. Typically, the beam signal is sampled every 20 msec for a total scan length of 2 sec; the electron gun is turned on at the center of the scan, $t = 1$ sec. A single run at a given electron energy consists of 960 succesive scans, accumulating the sampled signal time channel by time channel. At the end of 960 scans, the data accumulation is stopped, and the computer performs a least-squares linear fit to both halves of the data, the first half with the electron gun off and the second half with the electron gun on. With the results of these fits, $\Delta I/I_0$ at $t = 1$ sec is computed and then a value for the observed cross section $\bar{\sigma}$ is produced by using Eq. (3).

Precise tuning of the laser to the atomic transition is maintained by constantly monitoring the atomic beam with the electrometer and correcting the laser frequency manually when necessary.

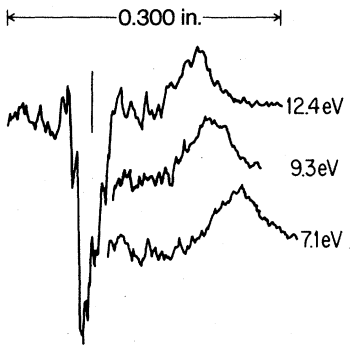

FIG. 5. Atomic beam signal with detector moving parallel to electron beam, at three different electron energies. The prominent positive peaks are the forward inelastic scattering peaks. The negative peak indicates scattering off the atomic beam. The vertical line above it marks the position of the center of the beam.

V. PHOTON-RECOIL RESULTS

Figure 6 shows the atomic beam detector signal as a function of laser frequency, with the detector

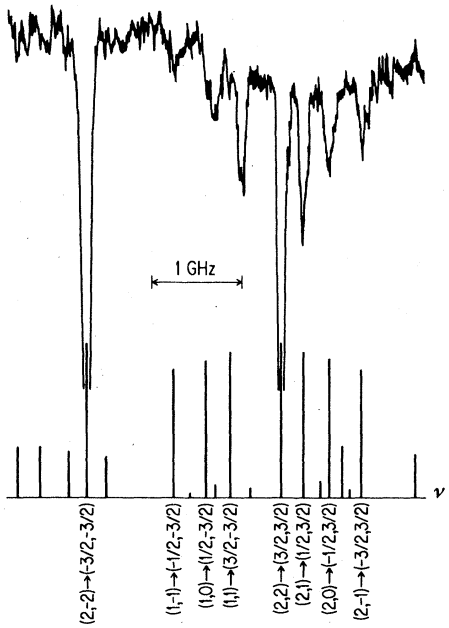

FIG. 6. Atomic beam signal as a function of laser frequency. The detector is on axis, and the beam is unpolarized. The vertical lines at the bottom mark calculated positions and intensities of all the transitions allowed in the frequency interval being scanned. We have labeled only the eight most intense lines, using the $(F,m) \rightarrow (m_I, m_J)$ notation.

on the beam axis. The negative peaks occur at the frequencies at which atoms are recoiled off axis by resonant photon interactions. The atomic beam in this case is unpolarized; that is to say, all eight hyperfine sublevels of the ground state are present.

In the same figure we have plotted the theoretical absorption lines. The positions of the lines were computed by using the hyperfine and Zeeman energy shifts for the ground and excited states, $\delta\nu_S$ and $\delta\nu_P$, respectively.

For the $3\,^2S_{1/2}$ state we are in an intermediate-field case, so that the Breit-Rabi formula was used. For sodium, for which $I=\frac{3}{2}$, we have

$$\delta\nu_S(F,m) = -\tfrac{1}{8}\Delta W \pm \tfrac{1}{2}\Delta W(1+mx+x^2)^{1/2}, \qquad (15)$$

where x is the dimensionless Rabi parameter defined in Sec. III and $\Delta W = 1771.63$ MHz is the ground-state hyperfine splitting.

For the $3\,^2P_{3/2}$ state we are in a high-field case, so that

$$\delta\nu_P(m_J, m_I) = m_J y + A m_J m_I, \qquad (16)$$

where $A = 19.06$ MHz is the hyperfine splitting of the $3\,^2P_{3/2}$ state and $y = g'_J \mu_B H/h$ (g'_J is the gyromagnetic factor of this state).

We calculated the strengths of the transitions using the uncoupled representation $|m_I, m_J\rangle$ for both the excited and the ground states. For the excited state we can simply write

$$|k\rangle = |m'_I, m'_J\rangle, \qquad (17)$$

since it is in a high-field regime. For the ground state, since it is in an intermediate-field regime, we write, for levels with $|m| \neq I+J$,

$$|s\rangle = \mathfrak{A}_{F,m}(H)\,|m-\tfrac{1}{2}, \tfrac{1}{2}\rangle + \mathfrak{B}_{F,m}(H)\,|m+\tfrac{1}{2}, -\tfrac{1}{2}\rangle. \qquad (18)$$

On the other hand, if $m = \pm(I+J)$, we write

$$|s\rangle = |\pm I, \pm J\rangle. \qquad (19)$$

The transition strengths will be, for $|m| \neq I+J$,

$$T_{s,k} \propto (\delta_{m'_I, m-1/2}\,|\mathfrak{A}|^2\,|\langle \tfrac{1}{2}, 1, \tfrac{1}{2}, m'_J - \tfrac{1}{2}\,|\,\tfrac{1}{2}, 1, \tfrac{3}{2}, m'_J\rangle|^2 + \delta_{m'_I, m+1/2}\,|\mathfrak{B}|^2\,|\langle \tfrac{1}{2}, 1, -\tfrac{1}{2}, m'_J + \tfrac{1}{2}\,|\,\tfrac{1}{2}, 1, \tfrac{3}{2}, m'_J\rangle|^2)\,|\langle \alpha', J'\|x\|\alpha, J\rangle|^2, \qquad (20)$$

and for $m = \pm(I+J)$ they will be

$$T_{s,k} \propto \delta_{m'_I, \pm I}\,|\langle \tfrac{1}{2}, 1, \pm\tfrac{1}{2}, \Delta m_J\,|\,\tfrac{1}{2}, 1, \tfrac{3}{2}, m'_J\rangle|^2 \times |\langle \alpha', J'\|x\|\alpha, J\rangle|^2. \qquad (21)$$

As we are interested only in the relative strengths of the transitions, we can leave out the reduced matrix element $\langle \alpha', J'\|x\|\alpha, J\rangle$. The field-dependent coefficients $\mathfrak{A}_{F,m}(H)$ and $\mathfrak{B}_{F,m}(H)$ can be calculated by using Torrey's[35] results. Torrey calculated the field-dependent state vectors $|I \pm \frac{1}{2}, m; H\rangle$ in the coupled representation $|F, m\rangle$, obtaining

$$|I \pm \tfrac{1}{2}, m; H\rangle = A_{F,m}\,|I+\tfrac{1}{2}, m\rangle + B_{F,m}\,|I-\tfrac{1}{2}, m\rangle. \qquad (22)$$

Using

$$|F, m\rangle = \sum_{m_I, m_J} |m_I, m_J\rangle\langle I, J, m_I, m_J\,|\,I, J, F, m\rangle, \qquad (23)$$

we can calculate $\mathfrak{A}_{F,m}(H)$ and $\mathfrak{B}_{F,m}(H)$ in terms of Torrey's coefficients $A_{F,m}(H)$ and $B_{F,m}(H)$.

If we compare the signal with the theoretical absorption lines in Fig. 6, we can see that the beam intensity is decreased much more drastically by the transitions which do not depopulate their ground states, $(2,-2) \rightarrow (-\frac{3}{2}, -\frac{3}{2})$ and $(2,2) \rightarrow (\frac{3}{2}, \frac{3}{2})$, than for the other six transitions of comparable strength, which do. This is because the number of photons absorbed per atom will be much larger if the transition does not depopulate its ground state.

A typical vertical beam profile with the laser tuned to one of the two useful transitions is shown in Fig. 7 together with the corresponding profile with the laser off. The intensity of the difference

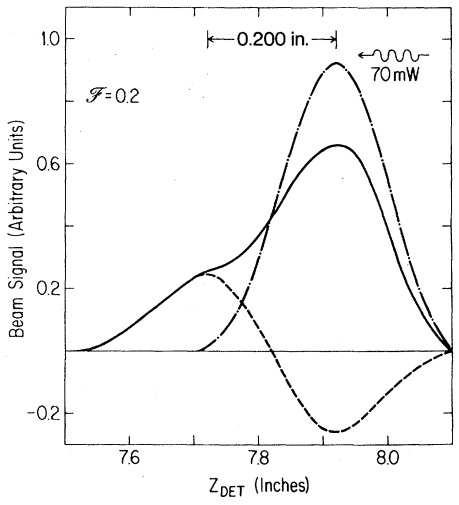

FIG. 7. Solid line shows the vertical beam profile with the laser tuned to a nondepopulating transition. The atomic beam is polarized. The laser power (measured at the laser output) was 70 mW. The long-dashed line shows the vertical beam profile with the laser off. The short-dashed line is the difference signal.

signal peak ("excited-state beam") is about 25% of the intensity of the beam with the laser off. This is fully consistent with an atomic beam consisting of four equally populated hyperfine states and shows that virtually every atom available for excitation by the laser is being excited many times.

From the deflection of the excited-state beam, $d = 0.200$ in., we calculate $\mathfrak{F} = 0.2$, which is a typical value for our experiments. This value of $\mathfrak{F}$ corresponds to $\rho = \frac{1}{3}$. The average number of spontaneous decays per atom during the transit time τ is $N \simeq 280$. About 370 photons per atom are absorbed from the laser beam. The average accumulated first-order Doppler shift will be about 14 MHz, which is not negligible. Actually this Doppler shift may have been a factor preventing us from obtaining higher values of $\mathfrak{F}$.

Horizontal beam profiles of the excited-state beam and the atomic beam with the laser off are shown in Fig. 8. As these profiles are obtained with the detector being translated perpendicularly to the laser beam, no relative displacement of both atomic beams should be observed; this is indeed the case. What one can observe is a broadening of the excited-state beam relative to the primary one. This broadening is about 0.004 in. (14%), which is in good agreement with the result predicted by Eq. (12).

VI. TOTAL SCATTERING CROSS SECTION

In order to take scattering data for the $3\,^2P_{3/2}$ state, the detector is set at about 0.200 in. below the beam axis, where the excited-state beam signal peaks. At this position the contribution to the signal from the 75% of the atoms which are not excited by the laser is negligibly small.

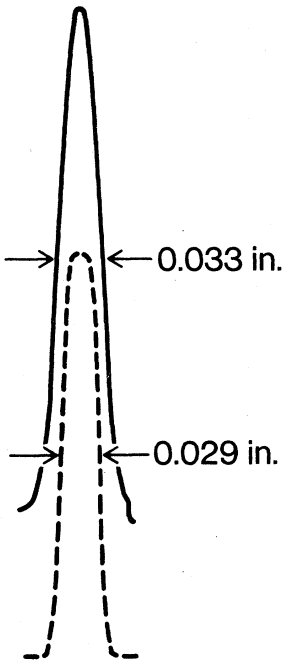

FIG. 8. Solid line shows the horizontal beam profile with the laser tuned to a nondepopulating transition, while the dashed line shows the horizontal beam profile with the laser off. The width of the beam with the laser off is 0.029 in. (FWHM). The beam with the laser on is broadened to 0.033 in (FWHM).

For a given electron energy the observed cross section for electron scattering by the mixture of ground- and excited-state atoms present in the interaction region is given by Eq. (3). The atomic-beam velocity V, the electron current I_e, and the scattering-off signal $\Delta I/I_0$ are determined as discussed in Sec. IV. The height of the atomic beam is defined by a mask that was carefully measured under a travelling microscope to be $h_A = 0.1632 \pm 0.0003$ cm. Figure 9 shows the raw data for a typical run, as well as the results of the computer fit for the atomic beam signals at $t = 1$ sec (when the electron gun is turned on), I_{off} and I_{on}, from which the scattering-off signal $\Delta I/I_0$ is computed. Typical errors for the scattering-off signal are about 5%. The error in determination of the observed cross section $\bar{\sigma}$, after propagating the errors affecting the other quantities in Eq. (3), will be about 8%.

We derive the excited-state total cross sections from the values of $\bar{\sigma}$ using Eq. (4). The excited-state fraction $\mathfrak{F}$ is determined by means of Eq. (11), with the length of the interaction region (defined by suitably placed masks) $l = 3.17 \pm 0.03$ cm.

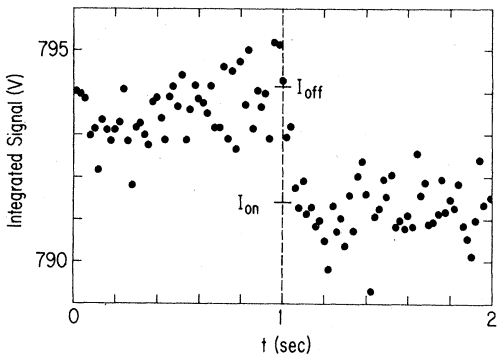

FIG. 9. Typical raw-data set, accumulated at the computer after 960 2-sec scans. The beam signal is sampled at 20-msec intervals. The electron gun is turned on at $t = 1$ sec and off at $t = 2$ sec, after which a new scan is started; I_{on} and I_{off} are obtained from linear least-squares fits to both halves of the data. The scattering-off signal is $\Delta I = I_{\text{off}} - I_{\text{on}} = 2.73 \pm 0.14$ V, while the beam signal with the electron gun off is $I_0 = 794.12 \pm 0.09$ V. The corrected electron energy in this case is 1.1 eV; the atomic beam velocity is 965 ± 27 m/sec. From these values one obtains $\bar{\sigma} = (2.17 \pm 0.13) \times 10^{-14}$ cm^2 for the observed total cross section for the scattering of electrons by the mixture of ground and excited sodium atoms. The excited-state fraction in this case is $\mathfrak{F} = 16\%$.

The error introduced in $\mathfrak{F}$ by the photon statistics, as discussed in Sec. III, is about 6%. After propagating the errors affecting the other quantities intervening in Eq. (11), we find the net error in $\mathfrak{F}$ is about 15%. Equation (4) requires the use of the ground-state cross sections; we have used the values of Kasdan *et al.*[11] The main contributions to the error in the excited-state cross sections are those of $\mathfrak{F}$ and σ. The latter is the largest, owing to its high propagation factor. The contribution from the error in the ground-state cross section is very small. The total error in a single determination of the excited-state cross section using Eqs. (3) and (4) is about ±35%.

Several (typically eight) measurements of the excited-state cross sections as outlined above were performed at each electron energy. The observed statistical spread of the measurements was consistent with the ±35% error estimate for a single measurement discussed above. Our results are presented in Fig. 10 as averages and standard errors computed from each set of measurements.

The results of the calculations of Moores *et al.*[23] presented in Table I of their paper cannot be compared directly to our experimental results, since they are the particular combinations of T-matrix elements which describe the scattering of electrons by a sodium target in which all the $3P$ states are populated. If the elements of the T matrix are available, it should be straightforward to compute the cross sections relevant to our experiment.

The consistency between the standard deviation estimated for a single measurement and the statistical spread of a group of measurements for a single electron energy does not preclude the possible presence of systematic errors. These can be divided into two groups: those affecting the determination of the energy scale and the measurement of σ, which can be tested by ground-state diagnosis, and the others affecting the determination of $\mathfrak{F}$, which cannot be tested in this way.

In order to check the first group, we performed measurements of the total cross section for electron scattering by ground-state sodium. These measurements have been performed under conditions resembling as closely as possible those used for the excited state. Equation (3) was used to compute the cross sections, employing the procedure previously outlined to measure $\Delta I/I_0$. This would have detected any systematic errors in the velocity determination, the measurement of the electron current, and the geometry of the overlap between electron and atomic beams, as well as any nonlinearity in the energy scale due to space charge in the interaction region, and energy shifts due to incorrect determination of contact potential differences. The results are presented in Fig. 11, and they are in excellent agreement with the results of Kasdan *et al.*[11] as well as the four-state close-coupling calculations of Moores and Norcross.[21]

Separate checks were performed to test the operation of the electron gun. In order to test the accuracy of the space-charge correction to the electron energy, we measured the ground-state total scattering cross section as a function of electron-gun current, varying the electron-gun voltages in the manner required by the space-charge correction to keep the electron energy

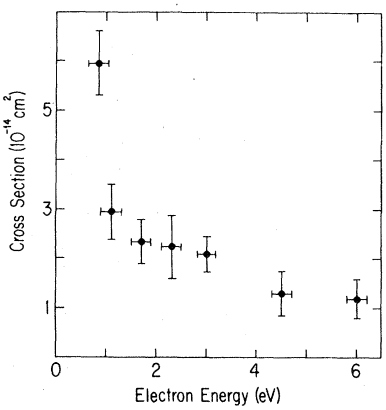

FIG. 10. Total cross sections for the scattering of electrons by $3P_{3/2}$ sodium atoms. Black dots represent the results of the present work. Horizontal error bars give the electron energy spread; vertical bars reflect statistical errors.

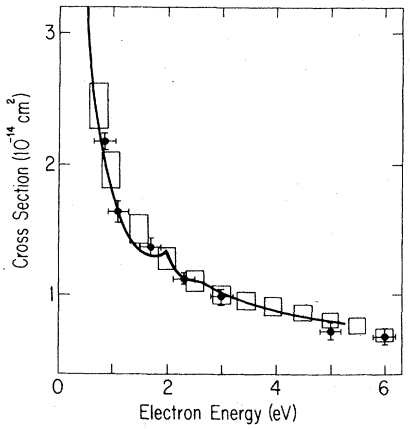

FIG. 11. Total cross sections for the scattering of electrons by ground-state sodium atoms. Black dots represent the results of the present work. Horizontal error bars give the electron energy spread; vertical bars reflect statistical errors. Rectangles represent the measurements by Kasdan *et al.*[11]; solid line, the four-state close-coupling calculation by Moores and Norcross.[21]

fixed in the interaction region. Figure 12(a) shows the results for $E = 3$ eV, and as expected, the measured cross section is independent of electron-gun current, or equivalently, the scattering signal is linear with the electron current. In a second test we measured the ground-state scattering cross section as a function of applied anode voltage, at fixed electron energy and current. Figure 12(b) shows the results for $E = 1.90$ eV, $i = 70$ μA. It is apparent that at low anode voltages the presence of electrons backscattered from the anode increases the effective electron current in the interaction region, leading to a serious overestimation of the cross section, but at higher voltages the effect is not important; our operating anode voltage was 50 V.

The possible sources of systematic error affecting the determination of $\mathfrak{F}$ are the measurement of the atomic beam velocity, which was checked in relation to the first group of systematic error sources, and a lack of complete overlap between the atomic, electron, and laser beams. If a significant volume of the region in which electrons and atoms interact were not illuminated by the laser, the value of $\mathfrak{F}$ obtained by using Eq. (11) would be larger than the effective fraction of excited atoms in the entire volume of the interaction region. But we have strong evidence that this was not the case. We know that there was full overlap between the laser and atomic beams, because 25% of the atoms in the beam were in the ground-state sublevel that could be excited by the laser and 25% of the atoms in the beam were deflected down by photon recoil. As for the overlap between the electron and laser beams, visual inspection showed that the laser beam illuminated the whole width of the ribbonlike electron beam.[36]

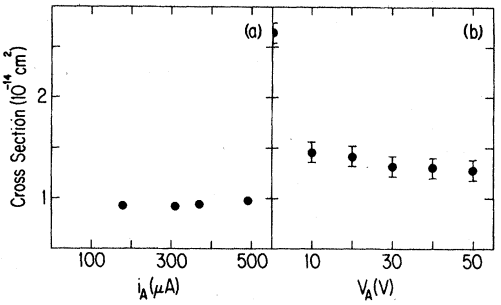

FIG. 12. Electron beam diagnostics. (a) Measured ground-state cross section vs electron-gun current, at the fixed electron energy $E = 3.00$ eV (after correction for space charge). (b) Measured ground-state cross section as a function of the voltage applied at the anode of the electron gun. The electron energy is $E = 1.90$ eV; the gun current is $i = 70$ μA.

In sum, we believe that the standard errors represented in Fig. 10 are the only significant errors affecting our determination of the total cross section for electron scattering by sodium atoms in the $3\,^2P_{3/2}$, $m_J = \pm\frac{3}{2}$ state.

ACKNOWLEDGMENTS

We thank Dr. David Norcross for pointing out to us the differences between the calculations in the paper by Moores *et al.*[23] and our experiment. We also thank Mr. Neil Pignatano for his help in programming the DECLAB-03 computer, and Professor Howard H. Brown, Jr. for his gracious offer of a pump laser when ours failed during the last stages of the experiment. This research was supported in part by the National Science Foundation.

*Present address: Joint Institute for Laboratory Astrophysics, Univ. of Colorado, Boulder, Col. 80302.
[1]R. Celotta, H. Brown, R. Molof, and B. Bederson, Phys. Rev. A 3, 1622 (1971).
[2]G. M. Carter, D. E. Pritchard, M. Kaplan, and T. W. Ducas, Phys. Rev. Lett. 35, 1144 (1975).
[3]R. Düren, H. O. Hoppe, and H. Pauly, Phys. Rev. Lett. 37, 743 (1976).
[4]I. V. Hertel and W. Stoll, J. Phys. B 7, 583 (1974); H. W. Hermann, I. V. Hertel, W. Reiland, A. Stamatovic, and W. Stoll, *ibid.* 10, 251 (1977).
[5]N. D. Bhaskar, B. Jaduszliwer, and B. Bederson, Phys. Rev. Lett. 38, 14 (1976).
[6]S. Trajmar (private communication).
[7]J. Macek and I. V. Hertel, J. Phys. B 7, 2173 (1974).
[8]I. V. Hertel and W. Stoll, in *Advances in Atomic and Molecular Physics*, edited by D. R. Bates and B. Bederson (Academic, New York, 1977), Vol. 13, pp. 113–128.
[9]P. J. Visconti, J. A. Slevin, and K. Rubin, Phys. Rev. A 4, 1310 (1971); J. A. Slevin, P. J. Visconti, and K. Rubin, *ibid.* 5, 2065 (1972).
[10]R. E. Collins, B. Bederson, and M. Goldstein, Phys. Rev. A 3, 1976 (1971).
[11]A. Kasdan, T. M. Miller, and B. Bederson, Phys. Rev. A 8, 1562 (1973).
[12]W. Gehenn and M. Wilmers, Z. Phys. 244, 395 (1971).
[13]D. Andrick, M. Eyb, and M. Hoffman, J. Phys. B 5, L15 (1972).
[14]D. Hils, M. V. McCusker, H. Kleinpoppen, and S. J. Smith, Phys. Rev. Lett. 29, 398 (1972).
[15]R. E. Collins, M. Goldstein, B. Bederson, and K. Rubin, Phys. Rev. Lett. 19, 1366 (1967).
[16]B. Bederson and T. M. Miller, in *International Symposium on Electron and Photon Interactions with Atoms, University of Stirling, Scotland, 1974* (Plenum, New

York, in press).
[17]K. Rubin, B. Bederson, M. Goldstein, and R. E. Collins, Phys. Rev. 182, 201 (1969).
[18]M. Goldstein, A. Kasdan, and B. Bederson, Phys. Rev. A 5, 660 (1972).
[19]E. M. Karule, in *Atomic Collisions III*, edited by V. Ia. Veldre (Latvian Academy of Science, Riga, 1965), pp. 29–48; E. M. Karule and R. K. Peterkop, *ibid.*, pp. 1–27; E. M. Karule, J. Phys. B 5, 2051 (1972).
[20]D. W. Norcross, J. Phys. B 4, 1458 (1971).
[21]D. L. Moores and D. W. Norcross, J. Phys. B 5, 1482 (1972).
[22]These discrepancies have been discussed by Bederson and Miller (Ref. 16).
[23]D. L. Moores, D. W. Norcross, and V. B. Sheorey, J. Phys. B 7, 371 (1974).
[24]B. Jaduszliwer, R. Dang, P. Weiss, and B. Bederson, in *Coherence and Correlations in Atomic Collisions*, edited by H. Kleinpoppen and J. F. Williams (Plenum, New York, in press).
[25]For detailed descriptions of the apparatus and experimental techniques, see R. Dang, Ph.D. thesis, New York University, 1979 (unpublished).
[26]K. Rubin, J. Perel, and B. Bederson, Phys. Rev. 117, 151 (1960).
[27]This is the value of the magnetic field (parallel to the electron momentum) in the interaction region of our atomic-beam apparatus.
[28]J. I. Gersten and M. H. Mittleman, Phys. Rev. A 13, 123 (1976).
[29]M. H. Mittleman, Phys. Rev. A 14, 1338 (1976); 16, 1549 (1977).
[30]Hertel and Stoll (Ref. 7, pp. 131–133) show that this test is too restrictive and can be relaxed considerably while still maintaining the validity of the perturbation theory approach.
[31]O. Frisch, Z. Phys. 86, 42 (1933).
[32]S. Chandrasekhar, Rev. Mod. Phys. 15, 1 (1943).
[33]Düren *et al.* [*Festschrift* 50 *Jahre Max Planck-Institut für Strömungforschung* (MPI *für Strömungforschung, Göttingen*, 1975), pp. 414–428] studied carefully the deflection of a well-collimated, velocity-selected sodium beam by laser pumping.
[34]R. E. Collins, B. B. Aubrey, P. N. Eisner, and R. J. Celotta, Rev. Sci. Instrum. 41, 1403 (1970).
[35]E. C. Torrey, Phys. Rev. 59, 293 (1941).
[36]It should be pointed out that having the laser beam illuminate a volume larger than the overlap between electron and atomic beams will not introduce a systematic error.